# Filtering and Thresholding the Analytic Signal Envelope in order to improve Peak and Spike Noise Reduction in EEG Signals

Umberto Melia *, Francesc Clariá **, Montserrat Vallverdú *, Pere Caminal *

*Dept. ESAII, Centre for Biomedical Engineering Research, Universitat Politècnica de Catalunya, CIBER of Bioengineering, Biomaterials and Nanomedicine (CIBER-BBN), Barcelona, Spain; email: umberto.melia@upc.edu, montserrat.vallverdu@upc.edu, pere.caminal@upc.edu.
**Dept. IIE, Lleida University, Spain; email: claria@diei.udl.es

*Total word count*: 3443words

ABSTRACT

To remove peak and spike artifacts in biological time series has represented a hard challenging in the last decades. Several methods have been implemented mainly based on adaptive filtering in order to solve this problem. This work presents an algorithm for removing peak and spike artifacts based on a threshold built on the analytic signal envelope. The algorithm was tested on simulated and real EEG signals that contain peak and spike artifacts with random amplitude and frequency occurrence. The performance of the filter was compared with commonly used adaptive filters. Three indexes were used for testing the performance of the filters: Correlation coefficient ($\rho$), mean of coherence function ($C$) and rate of absolute error ($RAE$). All these indexes were calculated between filtered signal and original signal without noise. It was found that the new proposed filter was able to reduce the amplitude of peak and spike artifacts with $\rho > 0.85$, $C > 0.8$, $RAE < 0.5$. These values were significantly better than the performance of LMS adaptive filter ($\rho < 0.85$, $C < 0.6$, and $RAE > 1$).

*Keywords*: Biomedical signal processing, electroencephalography, digital filters.

## 1. Introduction

Electroencephalographic (EEG) signal is very susceptible to a variety of large signal contamination such as power line noise, biological or electrode artifacts. As these artifacts can be associated to cerebral activity they should be removed by filtering before further signal analysis. However, traditional methods, such as band-pass filter, are not adequate if the frequency band of the contaminant signal is within the band of the true signal, for example the electromyographic signal and the power line noise. There exist other kinds of artifacts that need different approaches to be removed, for example, certain peak and spike noise, heart electrical activity present throughout the body [1], short-time high-amplitude events in the recorded EEG for the evaluation of epileptic seizures that mask the quasi-periodic structure of the seizures [2]. The most commonly used approaches for these problems are filters mainly based on adaptive algorithms with linear and nonlinear structures [3, 4] or eigenvalue decomposition [5]. Furthermore, eye blinks and movements of the eye balls produce electrical activity along the scalp that interferes with the EEG. In order to remove ocular artifacts from EEG, many regression-based techniques have been proposed [6-11]. They require calibration trials in order to estimate the electrooculogram (EOG) component from each one of the EEG channels and then they remove it by subtraction. Independent component analysis (ICA) represents an efficient way [12, 13] to perform EOG signal separation from the EEG signals. Several methods for dealing with ocular artifacts in the EEG were reviewed by Croft et *al.* [14], focusing on the relative merits of a variety of EOG correction procedures. A noise cancellation method based on adaptive filtering was implemented by He et *al.* [15] with the aim of removing ocular artifacts from on-line EEG without calibration trials but using the EOG signal as reference. Furthermore, the acquisition of EEG during functional magnetic resonance imaging (fMRI) procedure is contaminated by numerous possible sources of artifacts, such as short-time and high-amplitude events for instance burst suppression, artifacts originated from the surrounding electromagnetic field, the fMRI-related gradient artifacts, and cardiac pulse interference [16]. These are induced effects due to alterations in the magnetic field gradient [17-20]. Artifacts induced in EEG recordings by electrical impedance tomography (EIT) are analogous to those generated by interictal spike-triggered fMRI during simultaneous EEG and fMRI monitoring. In order to remove EIT artifacts, Fabrizi et *al.* [21] used a bank of hardware filter (first-order passive high-pass filters and second-order passive low-pass filters) associated with a digital filter based on a single template of the EIT noise. A new methodology to reduce these artifacts was proposed by Melia et *al.* [22] where a filter based on the analytic signal envelope was designed. This filter can be applied to each single-channel recording without using any reference signal. In the present work, an improvement of the filter algorithm is presented, that consists in introducing a threshold calculated on the analytic signal envelope. The algorithm was tested using simulated and real EEG

signals corrupted by noise with peaks and spikes of high amplitude. Spike refers to sharp impulses of linearly rising and falling edges with a pointed peak and duration of about 80 ms. Peak refers to an isolated event with value out of the range of the signal variance.

## 2. Materials and Methods

### 2.1 The Hilbert Transform and the Analytic Signal

The Hilbert transform $\hat{x}(t)$ is a linear function of a signal $x(t)$. It is obtained from the convolution of $x(t)$ with $(\pi\ t)^{-1}$ [23, 24]. The analytic signal $y(t)$ of a real signal $x(t)$ can be written as

$$y(t) = x(t) + j\hat{x}(t) = m(t)\cos\big(\phi(t)\big) + j\,m(t)\sin\big(\phi(t)\big) \tag{1}$$

where $x(t)$ can be expressed as the product of two signals

$$x(t) = m(t)\cos(\phi(t)) \tag{2}$$

Expression (2) shows that $x(t)$ can be modified in two different ways, by varying the amplitude $m(t)$ and/or by varying the phase $\phi(t)$. The simultaneous dual behavior of $x(t)$ in amplitude and frequency modulation suggests that changes in the signal amplitude leave its zero crossings unchanged. Therefore, the aim of this procedure is to modify the amplitude without altering the components that could cause the zero crossings on the time axis.

The contribution of the amplitude $B_{AM}^2$ and phase $B_{FM}^2$ of a signal to its bandwidth [24] is defined by (3-5), where $m(t)^2 = |y(t)|^2 = y(t)\,y^*(t)$ is the instantaneous power or energy density (see Appendix).

$$B^2 = B_{AM}^2 + B_{FM}^2 \tag{3}$$

where $B$ is the total bandwidth of the signal $x(t)$

$$B_{AM}^2 = \frac{1}{4\pi^2}\int \left(\frac{m(t)'}{m(t)}\right)^2 m(t)^2 dt \tag{4}$$

$$B_{FM}^2 = \int \big(f_i(t) - \bar{f}\big)^2 m(t)^2 dt \tag{5}$$

where $m(t)'$ is the derivative of the analytic signal envelope $m(t)$, $f_i(t) = \frac{1}{2\pi}\frac{d\phi(t)}{dt}$ is the instantaneous frequency function and $\bar{f}$ is the mean frequency of the spectral density of $y(t)$.

The term $B_{AM}^2$ associated with the analytic signal amplitude contributes to the low frequencies of $B$ and the term $B_{FM}^2$ associated with the analytic signal phase contributes to the high frequencies of $B$. In this way, the expression $B_{AM}$ determines the bandwidth with which $m(t)$ contributes to the signal $x(t)$ and thus it adjusts the bandwidth of a filter that applied to $m(t)$ removes the peaks and spikes from $x(t)$.

### 2.2 Description of the Filter Algorithm

The proposed algorithm consists of an analytic signal envelope filtering (ASEF) that reduces the amplitude of peaks or spikes in the EEG signals. Firstly, the envelope $m(t)$ of a signal $x(t)$ is filtered using a low-pass filter with a pass band $B_{AM}$, then a threshold $Th(t)$ based on the filtered envelope $m_{filt}(t)$ is defined and finally this threshold is applied to the envelope $m(t)$. This $Th(t)$ is calculated at each time sample of $m_{filt}(t)$ as

$$Th(t) = m_{filt}(t) + k\,\overline{m_{filt}} \tag{6}$$

where $\overline{m_{filt}}$ is the mean value of $m_{filt}(t)$ and $k$ is an arbitrary constant.

The main steps of the proposed filter algorithm applied to a signal $x(t)$ are:
1) To calculate the analytic signal $y(t)$ of $x(t)$.

2) To calculate the envelope $m(t)$ and the instantaneous phase $\phi(t)$.
3) To filter the $m(t)$ by using a FIR filter with a cut off frequency $B_{AM}$ in order to obtain $m_{filt}(t)$.
4) To preserve the samples that satisfy $m(t) < Th(t)$ in order to obtain the signal $m_{Th}(t)$ (7).
5) To multiply the filtered envelope $m_{Th}(t)$ by $cos\phi(t)$, in order to obtain the final filtered signal $x_{filt}(t)$ (8).

$$m_{Th}(t) = \begin{cases} m_{filt}(t): & if \ m(t) \geq Th(t) \\ m(t): & if \ m(t) < Th(t) \end{cases} \tag{7}$$

$$x_{filt}(t) = m_{Th}(t)cos\phi(t) \tag{8}$$

This filter removes all or part of the peaks or spikes (depending on $k$ value of $Th(t)$) in the original signal $x(t)$, preserving its frequency information.

*2.3 Simulated Time Series*

A set of simulated time series $x(t)$ of EEG signals corrupted by peak or spike noise was generated.

$$x(t) = s(t) + n(t) \tag{9}$$

where $s(t)$ represents the pure EEG signal and $n(t)$ a signal containing random events of peak or spike waveforms.
The signals $s(t)$ were created by using functions that generate simulated EEG data [25]. These functions create uncorrelated noise generated such that its power spectrum matches the power spectrum of human EEG. The simulated EEG was constructed by summing together a number of phase-randomized sinusoids (frequencies from 0.1 to 125 Hz and phase between 0 and $2\pi$), the amplitude of which varied with frequency according to the power spectrum of empirical EEG data. Because this process amounts to an inverse-Fourier transform (with randomized phase) of a spectral analysis of real data, the simulated data match closely the features of empirically observed EEG data [26-27]. The mean value of $s(t)$ is $\overline{s(t)} = 0$ and the standard deviation is bounded $0.6 < \sigma_s < 1 \ \mu V$.
The noise $n(t)$ was created combining peak and spike events with random amplitude and random frequency of occurrence, in order to simulate the worsts noisy case in the EEG signal. The spike events were simulated with triangle waveforms, $tri(t)$

$$tri(t) = \begin{cases} \mu_{tri}(1 - |t - t_{tri}|): & if \ 0 \leq t \leq 2t_{tri} \\ 0: & otherwise \end{cases} \tag{10}$$

where $\mu_{tri}$ is a random variable that has normal distribution with expected value $\bar{\mu}_{tri} = 0$, standard deviation $20\sigma_s$, and $t_{tri} = 0.04$ s. These values permitted to create triangle waveforms with negative or positive values about 20 times the maximum EEG value and with duration that simulates short-time spike EEG artifacts. Then, the signal noise $n(t)$ was built as

$$n(t) = \begin{cases} tri(t - t_{n1}): & if \ t = t_{n1} \\ \mu_{peak}: & if \ t = t_{n2} \\ 0: & otherwise \end{cases} \tag{11}$$

where $\mu_{peak}$ is a random variable that has normal distribution with expected value $\bar{\mu}_{peak} = 0$ and standard deviation $20\sigma_s$, $t_{n1} \in T_1 = \{t_{11}, t_{21}, t_{31}, ..., t_{N1}\}$ and $t_{n2} \in T_2 = \{t_{12}, t_{22}, t_{32}, ..., t_{N2,}\}$, $\forall \ n = 1, 2, ..., N$ with $N = 40$. Where $t_{n1}$ and $t_{n2}$ are random variables with normal distribution and expected value $\bar{t}_{n1} = 50$ s and standard deviation $\sigma_{tn} = 50$ s. These values permitted to create noise events, with negative or positive values about 20 times the maximum EEG value, that occur between 0 s to 100 s with Gaussian distribution.
Two sets of 1000 signals $x(t)$ were generated with a sampling frequency of 256 Hz and a length of 100 s: set EEG1, 1000 signals corrupted with isolated peak and spike noise; set EEG2, 1000 signals corrupted with isolated peak and spike noise and with 20 consecutive triangle waveforms $(tri(t))$ in two randomly selected windows of 2 s along the signal. In this way, set EEG2 contains signals more contaminated than EEG1.

*2.4 Calculation of parameters $B_{AM}$ and $k$ of $Th(t)$*

In order to obtain the cutoff frequency value of the low-pass filter, equation (4) was applied to each signal $s(t)$ and $x(t)$ of the set EEG2, since it represents the worst case of noise. Then, the bandwidth $B_{AM}$ of the envelope $m(t)$ was calculated for each signal. The values of $B_{AM}$ are shown in Fig. 1 where the mean value of $B_{AM}$ is $\overline{B_{AM}} = 1.895 \pm 0.0514$ Hz for the signals $x(t)$ and $\overline{B_{AM}} = 0.9068 \pm 0.1068$ for the signals $s(t)$. This last value could represent the filter bandwidth value to theoretically eliminate all

134    peaks. In this way, a bandwidth of $B_{AM}$ =1 Hz can be an acceptable value and it was taken into account for the present study. In
135    the same way, the total bandwidth $B$ was calculated from the equation (3) obtaining a mean value $\bar{B}$= 57.44± 2.86 Hz for $x(t)$
136    signals and $\bar{B}$= 25.19± 3.00 Hz for $s(t)$ signals.
137
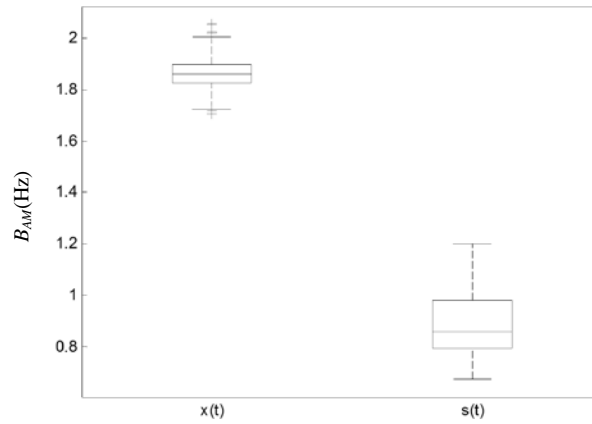


138

139    Fig.1 – Envelope bandwidth $B_{AM}$: signal $x(t)$ with noise ($\overline{B_{AM}}$= 1.895 ± 0.0514) and signal $s(t)$ without noise ($\overline{B_{AM}}$= 0.9068± 0.1068).
140

141    In order to find the best value of $k$ to calculate $Th(t)$ (6) that permits to have the best performance in peak and spike removal,
142    the ASEF algorithm was applied to the $x(t)$ signals of the set EEG2, varying $k$ in the $0.1 \leq k \leq 1.2$ range.
143    For each $x_{filt}(t)$ and $s(t)$ signal, the coherence function ($C_{xs}(f)$ ) and an index based on the rate of the absolute error ($RAE$)
144    before and after filtering were applied for validation.
145    $C_{xs}(f)$ [28] is a function of the power spectral densities ($P_{xx}$ and $P_{ss}$) and the cross power spectral density ($P_{xs}$) of $x(t)$ (or
146    $x_{filt}(t)$) and $s(t)$.
147

$$C_{xs}(f) = \frac{|P_{xs}(f)|^2}{P_{xx}(f)P_{ss}(f)} \tag{12}$$

148

149    where $0 \leq C_{xs}(f) \leq 1 \ \forall f$. The function $C_{xs}(f)$ indicates how well the signal $x(t)$ (or $x_{filt}(t)$) corresponds to $s(t)$ at each frequency $f$.
150    In this work, the index $C$ was defined as the mean value of $C_{xs}(f)$ with respect to $f$.
151    The index $RAE$ was defined as
152

$$RAE = \frac{E[|s(t) - x_{filt}(t)|]}{E[|s(t) - x(t)|]} \tag{13}$$

153

154    In this way, low values of $RAE$ denote low absolute error after filtering, indicating good efficiency in the removal of peak and
155    spike noise $n(t)$.
156    The optimum $k_b$ value was defined as the average of those $k$ values corresponding to the minimum $RAE$ and the maximum $C$.
157    For the set EEG2, $k_b$ = 0.43±0.07 is the optimum value (as seen in Fig. 2) and this is the value of $k$ that will be taken into account
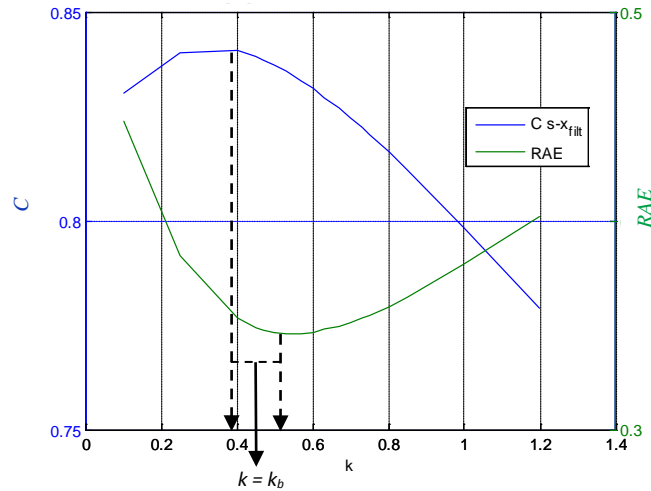158    in the present study.
159

Fig.2 – Mean value of *RAE* and *C* with respect to *k* for all *x*(*t*) signals of EEG2 set. The obtained *k* value is $k = k_b$=0.43.

### 2.5 Performance Test

In order to test the performances of the proposed ASEF algorithm and compare it with other filters [29-31], several known filters were applied to each simulated signal *x*(*t*) for obtaining a set of filtered signals $x_{filt}(t)$. These selected filters are:

- FIR (Finite Impulse Response) filter of 200th-order with a bandwidth of 0.1-30 Hz, since the calculated *B* value of *s*(*t*) signals is $\bar{B}$= 25.19± 3.00.
- LMS (Least Mean Square) adaptive filter of 500th-order with step size of 0.0001, using *s*(*t*) as reference signal.
- NLMS (Normalized Least Mean Square) adaptive filter of 300th-order with step size of 0.1, no leakage and using *s*(*t*) as reference signal.
- RLS (Recursive Least Square) adaptive filter of 100th-order, using *s*(*t*) as reference signal.

All parameters of the adaptive filters were chosen after several tests on a subset of simulated EEG data randomly chosen, in order to provide the highest correlation coefficient ($\rho$) and C and the lowest RAE, to guarantee filter stability with a reasonable computational cost.

The performances of ASEF filtering were evaluated using:

- ASEF without using the threshold *Th*(*t*) [22].
- ASEF using the threshold *Th*(*t*) with *k*=0.43.

In order to evaluate the performance of each filter, the correlation coefficient ($\rho$), *C* and *RAE* were calculated between signal $x_{filt}(t)$ and *s*(*t*).

### 2.6 Real EEG Data

Finally, ASEF was tested on real EEG data (*s*(*t*) signal). Noise signal *n*(*t*) was added to each signal *s*(*t*) and then the ASEF was applied to the corrupted signal *x*(*t*) (9).

The recordings *s*(*t*) belong to the EEG database that are available online by Andrzejak et al (2001) at the Department of Epileptology, University of Bonn (Germany) [32]. For the evaluation, two different subsets (A, B) were used, which contain surface EEG signals recorded from five healthy volunteers who were relaxed in the awaking state. Whereas the subjects had their eyes open during the recording of the EEG in subset A, the EEG signals of subset B were acquired with eyes closed. Each subset contains 100 single-channel EEG signals of 23.6 s, recorded with a sampling frequency of 173.6 Hz (4096 sample points).

## 3. Results

### 3.1 Simulated Time Series

The ASEF filtering reduces the amplitude of the peak and the triangular waveforms $n(t)$ without changing in a significant way the components of the pure signal $s(t)$. This effect can be observed in Fig. 3a where ASEF filtering was applied to a simulated corrupted signal $x(t)$. A segment of 5 seconds of the signal $x(t)$ and its corresponding filtered signal $x_{filt}(t)$ are shown in in Fig. 3b. In a similar way, Fig. 3c presents the same five-second segment of the $x(t)$ signal and its corresponding filtered signal $x_{filt}(t)$ by an adaptive filter LMS. Comparing Fig. 3b and Fig. 3c, it can be observed that ASEF filtering (Fig. 3b) and the adaptive filter (Fig. 3c) both present a reduction of the noise $n(t)$, but ASEF does not present any distortion of the $s(t)$ signal such as adaptive filter does.



(a)



(b)



(c)
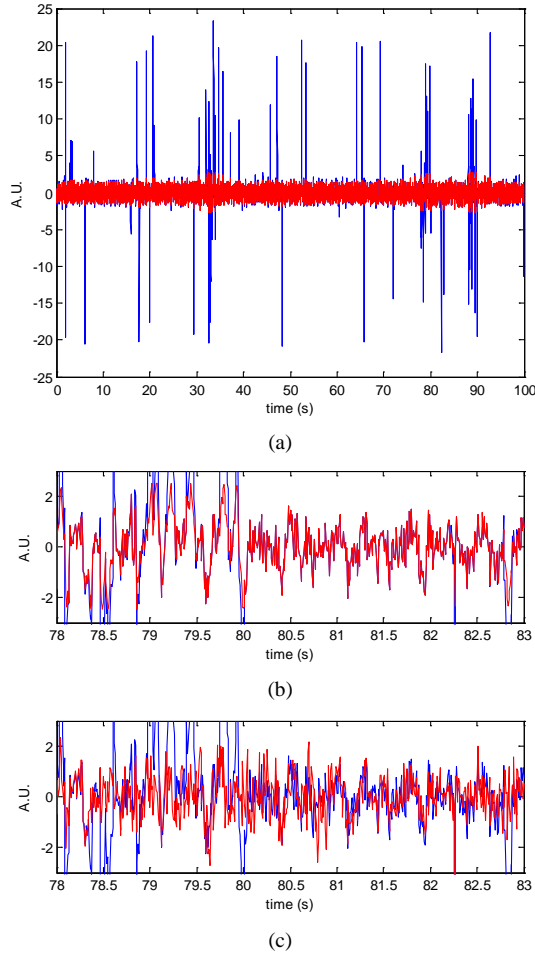
Fig. 3. (a) A simulated signal $x(t)$ with peaks and its filtered signal $x_{filt}(t)$ with ASEF filtering using the threshold $Th(t)$ with $k = 0.43$. (b) Zoom of 5 second segment of the $x(t)$ and $x_{filt}(t)$ signals. In red $x_{filt}(t)$, and in blue $x(t)$. (c) Zoom of 5 second segment of $x(t)$ and $x_{filt}(t)$ signals filtered with an adaptive filter LMS. In red $x_{filt}(t)$, and in blue $x(t)$.

Table 1 shows that the value of $\rho$ between $s(t)$ and $x_{filt}(t)$ was in the range of $0.5<\rho<0.85$ for the adaptive filters and the ASEF filtering without $Th(t)$. However, only the ASEF filtering with $Th(t)$ could obtain $\rho > 0.85$.

Table 1. Evaluation Performance: Pearson Correlation Coefficient ($\rho$)

| Filter | EEG1 (m±σ) |
|---|---|
| *ASEF TH k*=0.43 | 0.9085 ±0.0149 |
| *ASEF no TH* | 0.8283±0.0182 |
| *FIR* | 0.3839±0.0853 |
| *LMS* | 0.8075±0.0578 |
| *NLMS* | 0.7629±0.0643 |
| *RLS* | 0.5366±0.1562 |

*m, mean; σ, standard deviation*

Fig. 4 presents the boxplot of the $C$ and $RAE$ values calculated for all signals of EEG1 sets, in order to compare the performance of all filters. As it can be noted, ASEF filtering with $Th(t)$ gives the best values of the $RAE$ and the $C$.

225     The performance of the ASEF without $Th(t)$ was quite similar to the adaptive filters in terms of $RAE$ but present higher value
226    of $C$. Considering the performance of the best adaptive filter (LMS), it can be noted that even if the peak noise $n(t)$ is reduced,
227    the filtering affects also the pure signal $s(t)$ and consequently $RAE$ is higher in LMS than in ASEF and $C$ is lower in LMS than in
228    ASEF.



229
230                         (a)
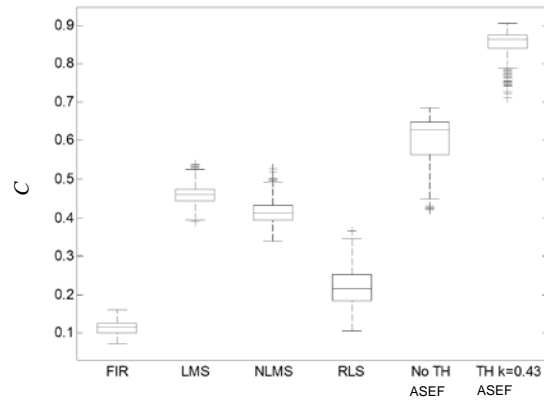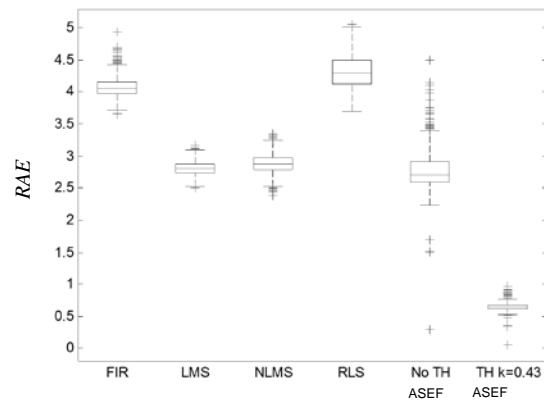


231
232                         (b)
233     Fig. 4. (a) Distribution of $C$ values and (b) distribution of $RAE$ values calculated for all simulated signals $x(t)$ of the EEG1 set. On each box, the central mark
234    is the median, the edges of the box are the 25th and 75th percentiles. The whiskers are lines extending from each end of the boxes to show the extent of the rest
235                      of the data. Values beyond the end of the whiskers are considered outliers and marked with a +.
236

237     *3.2 Real EEG data*

238

239     Fig. 5a shows an example of an EEG signal before and after ASEF filtering with $Th(t)$. The effect of the filtering was tested by
240    calculating the indexes $RAE$ and $C$ on unfiltered EEG, on EEG filtered with ASEF (without and with $Th(t)$) and on adaptive filter
241    (LMS). The LMS adaptive filter was chosen because it gave better performance than all other adaptive filters when applied to the
242    simulated dataset (as seen in Fig. 4). The results of $RAE$ and $C$ indexes calculated from $s(t)$ and $x_{filt}(t)$ are presented in Fig. 5b and
243    Fig. 5c. It can be observed a quite low value of $RAE$ and high value of $C$ when ASEF is applied with $k=0.43$. Also, it can be
244    noted that $RAE$ of LMS and ASEF without $Th(t)$ get values higher than the unit, that corresponds to non-filtered EEG ($x(t) =$
245    $x_{filt}(t)$). This means that filtering with these procedures introduces other type of noise to the original signal $s(t)$, consequently, the
246    absolute error value in the signal $x_{filt}(t)$ is higher than in the signal $x(t)$. The obtained values of $\rho$ between $s(t)$ and $x_{filt}(t)$ were
247    similar to those of simulated data: $0.55 < \rho < 0.85$ for the LMS and the ASEF filtering without $Th(t)$ and $\rho > 0.85$ for ASEF
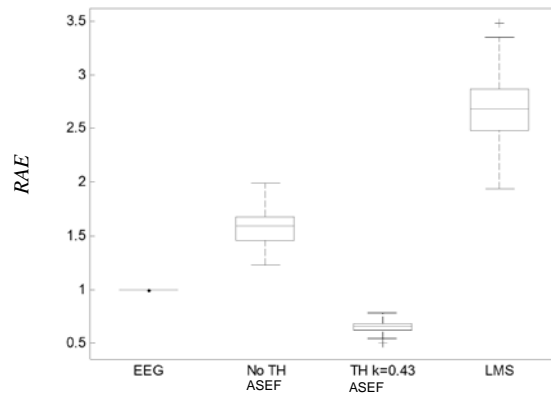248    filtering with threshold $Th(t)$.
249     These results denote a good performance in the removal of peaks and spikes also in real EEG data as well as in simulated EEG
250    data.
251
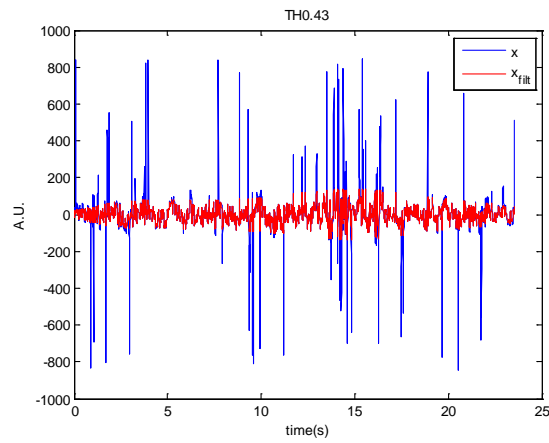
(a)
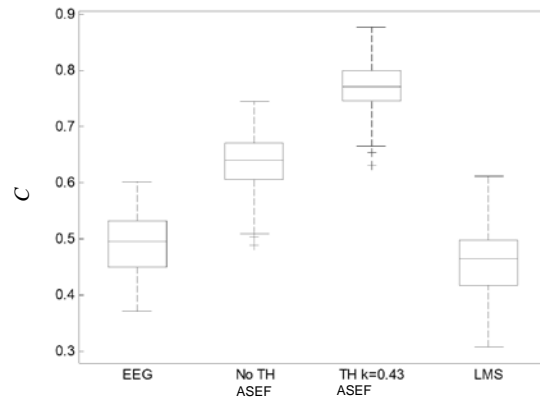
(b)

(c)

Fig. 5. (a) *x*(*t*) is a real EEG signal *s*(*t*) with peaks *n*(*t*) and $x_{filt}(t)$ is the filtered signal by using ASEF. (b) Distribution of $C$ values and (c) distribution of *RAE* values calculated between *x*(*t*) and the filtered $x_{filt}(t)$ in a set of 200 real EEG signals. EEG box represents the index calculated taken *x*(*t*) instead of $x_{filt}(t)$. On each box, the central mark is the median, the edges of the box are the 25th and 75th percentiles. The whiskers are lines extending from each end of the boxes to show the extent of the rest of the data. Values beyond the end of the whiskers are considered outliers and marked with a +.

*3.3 Uncorrupted signals*

Finally, the algorithm was applied to signals without any contamination. Table 2 shows $C$, *RAE* and $\rho$ values obtained applying *ASEF* with *k*=0.43 to all signals *s*(*t*) without any contamination, belonging to EEG1 set and real EEG data. In order to avoid division by zero in *RAE* calculation since *x*(*t*)=*s*(*t*), the denominator of the (13) was calculated using $x(t)=\overline{s(t)}$ where $\overline{s(t)}$ is the

263 mean value of s(t). Observing the values of Table 2 ($C$ >0.95, *RAE*<0.25 and  $\rho$ > 0.98), it can be deduced that the *ASEF* with
264 $k$=0.43 does not modify uncontaminated signals inappropriately.
265
266 Table 2. Evaluation Performance: $C$, *RAE* and Pearson Correlation Coefficient ($\rho$) for *ASEF* with $k$=0.43 applied to signals *s(t)*

| Index | EEG1 (m±σ) | real EEG (m±σ) |
|---|---|---|
| $C$ | 0.9561±0.0081 | 0.9721±0.0145 |
| *RAE* | 0.0659±0.0107 | 0.0568±0.0236 |
| $\rho$ | 0.9883±0.0025 | 0.9889±0.0056 |

267 *m, mean; σ, standard deviation*
268
269
270 ## 4.  Conclusions and Discussions
271
272 An algorithm for removing peak and spike noise from EEG is presented in this paper. This is based on filtering and
273 thresholding the analytic signal envelope. This filter preserves all information contained in the original signal phase, changing
274 only the bandwidth of the envelope. It was tested on a set of simulated and real EEG signals corrupted with peak and spike noise
275 *n(t)* and its performance was compared with adaptive filters calculating correlation coefficient ($\rho$), mean of coherence function
276 ($C$) and rate of absolute error (*RAE*).
277 Firstly, the optimum bandwidth $B_{AM}$ = 1 Hz of the envelope of a signal without peaks was calculated. Then applying $C$ and
278 *RAE* indexes, the optimum value of the parameter $k$ of the threshold *Th(t)* was calculated on a subset of simulated EEG signals,
279 obtaining $k$=0.43. Finally, using these values of $k$ and $B_{AM}$, the ASEF was applied on a dataset of simulated and real EEG signals
280 both corrupted with noise *n(t)*.
281 It can be noted from table 1 and Fig. 4 that ASEF with $k$= 0.43 has the highest $\rho$ and $C$ for both EEG1 and EEG2 sets; this
282 demonstrates the capability of the filter to retain the shape of the signal and also to preserve its frequency content.  These values
283 are even higher than the $\rho$ and $C$ of the best adaptive filter which was LMS filter. Furthermore, ASEF with $k$= 0.43 has the
284 lowest value of *RAE*. This means that ASEF with $k$= 0.43 has the best performance in reducing the noise without changing the
285 original signal for all the time of recording. The optimization of $B_{AM}$ and $k$ values will permit to preserve the episodes of
286 consecutive spikes with physiological information.
287 The results of the simulated signals were validated applying the ASEF algorithm to real EEG data corrupted by noise *n(t)*,
288 obtaining analogous performance results that simulated data. It has been demonstrated that this filter presents better performance
289 than adaptive filters applied to signals corrupted by non-periodic peak and spike noise. A remarkable feature of this filter is that
290 once the value of the parameters $B_{AM}$ and $k$ are obtained, for one kind of signal, it is not necessary to recalculate these parameters
291 for future filtering of the same physiological signal. The parameters $B_{AM}$ and $k$ calculated in this study have represented efficient
292 values for EEG signal, however different values of $B_{AM}$ and $k$ will permit to adapt the filter to the features of the different
293 physiological signals and noise situations.
294 The main aspect of the ASEF is that the amplitude of the signal *x(t)* is modified without changing the phase $\phi$(t) using only
295 the filtered envelope $m_{fill}(t)$. The filtered signal $x_{fill}(t)$ presents a reduction of the peak and spike amplitude compared with the
296 original signal *s(t)* (*RAE*<0.5), but without affecting the frequency components ($C$ >0.8). It should be noted that all this can be
297 calculated in the time domain without needing any reference signal or any multichannel recording. This is advantageous when it
298 is necessary to minimize the number of channels in a recording.
299 The concept and the methodology of this filter is similar to our previous designed filter published in [22], but in this current
300 paper the algorithm for the calculation of the bandwidth of the envelope at low frequencies of the generic signal was improved
301 and a threshold based on the filtered envelope was introduced. These modifications  have permitted to improve the performance
302 in terms of $C$, *RAE* and Pearson Correlation Coefficient ($\rho$). This new designed filter minimizes the inappropriate modification of
303 the original signal *s(t)*.The results have shown the capability of ASEF in reducing the noise, minimizing the absolute error rate
304 between filtered and pure signal in both simulated and real EEG data.
305

306 **Appendix**
307 The standard deviation $\sigma_f$, commonly known as bandwidth *B*, is defined as
308

$$B^2 = {\sigma_f}^2 = \int (f - \bar{f})^2 |Y(f)|^2 \, df = \overline{f^2} - \bar{f}^2 \tag{14}$$

309 where the spectral density $|Y(f)|^2$  is the Fourier transform of the autocorrelation function of the signal $y(t)$.
310 The time expression for the mean frequency can be calculated as

$$\bar{f} = \int f |Y(f)|^2 \, df = \frac{1}{j2\pi} \int j2\pi f \, Y(f)Y^*(f) df = \frac{1}{2\pi} \int y^*(t\ ) \frac{1}{j} \frac{dy(t)}{dt} dt \tag{15}$$

311

312 More specifically, if $y(t) = m(t)\,e^{j\phi(t)}$ then
313

$$\bar{f} = \frac{1}{2\pi} \int y^*(t) \frac{1}{j} \frac{dy(t)}{dt}\, dt = \frac{1}{2\pi} \int \frac{d\phi(t)}{dt} m(t)^2\, dt \qquad (16)$$

314
315 In similar way, the time expression of the mean square frequency is deduced as

$$\overline{f^2} = \int f^2\, |Y(f)|^2\, df = \frac{1}{(j2\pi)^2} \int j2\pi f\; Y(f)\; j2\pi f\; Y^*(f)df = \frac{1}{4\pi^2} \int \left|\frac{dy(t)}{dt}\right|^2 dt \qquad (17)$$

316
317 Then, the mean square frequency value for $y(t) = m(t)\,e^{j\phi(t)}$ is
318

$$\overline{f^2} = \frac{1}{4\pi^2} \int \left|\frac{dy(t)}{dt}\right|^2 dt = \frac{1}{4\pi^2} \int \left(\frac{dm(t)}{dt}\right)^2 dt + \frac{1}{4\pi^2} \int \left(\frac{d\phi(t)}{dt}\right)^2 m(t)^2 dt \qquad (18)$$

319
320 Finally, from the square of the signal bandwidth (14) in Hz and from the instantaneous frequency definition $f_i = \frac{1}{2\pi}\frac{d\phi(t)}{dt}$, the
321 following expression is obtained
322

$$B^2 = \frac{1}{4\pi^2} \int \left(\frac{m(t)'}{m(t)}\right)^2 m(t)^2 dt + \int \left(f_i(t) - \bar{f}\right)^2 m(t)^2 dt \qquad (19)$$

323
324 Consequently, the square bandwidth is made by a term that depends on the mean of the amplitude and another term that
325 depends on the mean of the frequency $B^2 = B_{AM}^2 + B_{FM}^2$.
326

## Acknowledgment

331

## Author Declaration

333 Competing interests: None declared
334 Funding:None
335 Ethical approval: Not required

336

## References

338
339 [1] Witte H, Glaser S, Rother M, New spectral detection and elimination test algorithms of ECG and EOG artefacts in neonatal EEG recordings. Med. Biol.
340 Eng. Comput. 1987; 25: 127-130.
341 [2] Celka P, Boashash B, Colditz P, Preprosessing and time-frequency analysis of newborn EEG seizures. IEEE Eng. Med. Biol. Mag. 2001; 20: 30–39.
342 [3] Haykin S, Adaptive Filter Theory. 3th Ed. Upper Saddle River: Prentice-Hall;1996.
343 [4] Lim SJ, Harris JG, Combined LMS/F algorithm. Electr. Lett. 1997; 33: 467-468.
344 [5] Hajipour S, Shamsollahi MB, Albera L, Merlet I, Noise cancelation of epileptic interictal EEG data based on generalized eigenvalue decomposition. 35th
345 International Conference on Telecommunications and Signal Processing (TSP) , 3-4 July 2012, pp. 591-595.
346 [6] Verleger R, Gasser T, Mocks J, Correction of EOG artifacts in event-related potentials of the EEG: Aspects of reliability and validity. Psychophysiology
347 1982; 19: 472-480.
348 [7] Gratton G, Coles MGH, Donchin E, A new method for off-line removal of ocular artifacts. Electroenceph. Clin. Neurophysiol. 1983; 55: 468-484.
349 [8] Kenemans JL, Molenaar ECM, Verbaten MN, Slangen JL, Removal of the ocular artifact from the EEG: A comparison of time and frequency domain
350 methods with simulated and real data. Psychophysiology 1991; 28: 115-121.
351 [9] Whitton JL, Lug E, Moldofsky H, A spectral method for removing eye movement artifacts from the EEG. Electroenceph. Clin. Neurophysiol. 1978; 44:
352 735-741.
353 [10] Woestenburg JC, Verbaten MN, Slanger JL, The removal of the eye-movement artifact from the EEG by regression analysis in the frequency domain.
354 Biological Psychology 1983; 16: 127-147.
355 [11] Veneri G, Federighi P, Rosini F, Federico A, Rufa A, Spike removal through multiscale wavelet and entropy analysis of ocular motor noise: A case study in
356 patients with cerebellar disease. Journal of Neuroscience Methods, 2011;196(2): 318-326.
357 [12] Jung TR, Makeig S, Westerfield M, Townsend J, Courchesne E, Sejnows TJ, Removal of eye activity artifacts from visual event-related potential in normal
358 and clinical subjects. Clin. Neurophysiol. 2000; 111: 1745-1758.

359 [13] LeVan P, Urrestarrazu E, Gotman J, A system for automatic artifact removal in ictal scalp EEG based on independent component analysis and Bayesian
360     classification. Clinical Neurophysiology 2006; 117(4): 912- 927.
361 [14] Croft RJ, Barry RJ, Removal of ocular artifact from the EEG: a review. Clinical Neurophysiology 2000; 30(1): 5–19.
362 [15] He PI, Wilson G, Russell C, Removal of ocular artifacts from electro-encephalogram by adaptive filtering Med. Biol. Eng. Comput. 2004; 42: 407-412.
363 [16] Allen PJ, Josephs O, Turner R, A method for removing imaging artifact from continuous EEG recorded during functional MRI. NeuroImage 2000; 12:
364     230–39.
365 [17] Huang C, Ju M, Lin C, A robust algorithm for removing artifacts in EEG recorded during FMRI/EEG study. Computers in Biology and Medicine,
366     2012;42(4): 458-467.
367 [18] Allen PJ, Polizzi G, Krakow K, Fish DR, Lemieux L, Identification of EEG events in the MR scanner: the problem of pulse artifact and a method for its
368     subtraction. Neuroimage 1998; 8: 229–39.
369 [19] Garreffa G, Real-time MR artifacts filtering during continuous EEG/fMRI acquisition. Magn. Reson. Imaging, 2003; 21: 1175–89.
370 [20] Sijbers J, Michiels I, Verhoye M, Van Audekerke J, Van der LA, Van Dyck D, Restoration of MR-induced artifacts in simultaneously recorded MR/EEG
371     data. Magn. Reson. Imaging 1999; 17: 1383–91.
372 [21] Fabrizi L, Yerworth R, McEwan A, Gilad O, Bayford R, Holder DS, A method for removing artifacts from continuous EEG recordings during functional
373     electrical impedance tomography for the detection of epileptic seizures. Physiol. Meas. 2010; 31: S57–S72.
374 [22] Melia USP, Claria F, Vallverdu M, Caminal P, Removal of Peak and Spike Noise in EEG Signals Based on the Analytic Signal Magnitude. Proceedings of
375     34th Annual International Conference of the IEEE Engineering in Medicine and Biology Society (EMBS) 2012; 3523-3526.
376 [23] Marple L, Computing the discrete-time "analytic" signal via FFT. IEEE Transactions on Signal Processing 1999; 47: 2600-2603.
377 [24] Cohen L, Time-frequency analysis. Prentice Hall Signal Processing Series; 1995.
378 [25] Yeung N, Bogacz R, Holroyd CB, Nieuwenhuis S, Cohen JD, Generation of simulated EEG data. Available from:
379     http://www.cs.bris.ac.uk/~rafal/phasereset/
380 [26] Yeung N, Bogacz R, Holroyd CB, Cohen JD, Detection of synchronized oscillations in the electroencephalogram: An evaluation of methods.
381     Psychophysiology 2004; 41: 822-832.
382 [27] Yeung N, Bogacz R, Holroyd CB, Nieuwenhuis S,  Cohen JD, Theta phase-resetting and the error-related negativity. Psychophysiology 2007; 44: 39-49.
383 [28] Stoica P, Moses R, Introduction to spectral analysis. Upper Saddle River; Prentice-Hall; 2005 pp.67-68.
384 [29] Farhang-Boroujeny B, Adaptive filters: Theory and applications. Chichester England: John Wiley & Sons; 1998.
385 [30] Proakis JG, Digital communications. 4th Ed. New York: McGraw-Hill; 2001.
386 [31] Shynk JJ, Frequency-domain and multirate adaptive filtering. IEEE Signal Processing Magazine 1992;9(1): 14-37.
387 [32] Andrzejak RG, Lehnertz K, Rieke C, Mormann F, David P, Elger CE, Indications of non-linear deterministic and finite dimensional structures in time series
388     of brain electrical activity: Dependence on recording region and brain state. Phys. Rev. E 2001; 64: 0619071–0619078.